

FedSemiDG: Domain Generalized Federated Semi-supervised Medical Image Segmentation

Zhipeng Deng^{a,b}, Zhe Xu^c, Tsuyoshi Isshiki^b and Yefeng Zheng^{a,*}

^aMedical Artificial Intelligence Lab, Westlake University, Hangzhou, China

^bDepartment of Information and Communication Engineering, School of Engineering, Institute of Science Tokyo, Tokyo, Japan

^cDepartment of Biomedical Engineering, The Chinese University of Hong Kong, Hong Kong, China

ARTICLE INFO

Keywords:

Domain Generalization
Federated Learning
Semi-supervised Learning
Medical Image Segmentation

ABSTRACT

Medical image segmentation is challenging due to the diversity of medical images and the lack of labeled data, which motivates recent developments in federated semi-supervised learning (FSSL) to leverage a large amount of unlabeled data from multiple centers for model training without sharing raw data. However, what remains under-explored in FSSL is the domain shift problem which may cause suboptimal model aggregation and low effectivity of the utilization of unlabeled data, eventually leading to unsatisfactory performance in unseen domains. In this paper, we explore this previously ignored scenario, namely domain generalized federated semi-supervised learning (FedSemiDG), which aims to learn a model in a distributed manner from multiple domains with limited labeled data and abundant unlabeled data such that the model can generalize well to unseen domains. We present a novel framework, Federated Generalization-Aware Semi-Supervised Learning (FGASL), to address the challenges in FedSemiDG by effectively tackling critical issues at both global and local levels. In our proposed framework, globally, we introduce **Generalization-Aware Aggregation (GAA)**, assigning adaptive weights to local models based on their generalization performance. Locally, we use a **Dual-Teacher Adaptive Pseudo Label Refinement (DR)** strategy to combine global and domain-specific knowledge, generating more reliable pseudo labels. Additionally, **Perturbation-Invariant Alignment (PIA)** enforces feature consistency under perturbations, promoting domain-invariant learning. Extensive experiments on three medical segmentation tasks (cardiac MRI, spine MRI and bladder cancer MRI) demonstrate that our method significantly outperforms state-of-the-art FSSL and domain generalization approaches, achieving robust generalization on unseen domains. This work provides a practical solution for addressing domain shifts in federated semi-supervised learning, advancing multi-center collaboration in privacy-sensitive healthcare applications. The code will be made public upon acceptance.

arXiv:2501.07378v1 [cs.CV] 13 Jan 2025

*Corresponding author

 deng.z.aa@m.titech.ac.jp (Z. Deng); jackxz@link.cuhk.edu.hk (Z. Xu); isshiki@ict.e.titech.ac.jp (T. Isshiki); zhengyefeng@westlake.edu.cn (Y. Zheng)

ORCID(s): 0009-0005-7602-5460 (Z. Deng); 0000-0002-1950-0959 (Z. Xu); 0000-0003-2195-2847 (Y. Zheng)

1. Introduction

Artificial intelligence (AI), particularly deep learning has gradually changed the landscape of computer-aided diagnosis (CAD), including medical image segmentation. The success of deep learning heavily relies on the availability of large-scale datasets. Due to stringent privacy regulations, however, it is difficult to collect large-scale medical image datasets from multiple centers for centralized learning, which hinders the development of medical AI. As a promising solution to this challenge, federated learning (FL) (McMahan et al., 2017) has drawn great attention in the healthcare domain, which enables multi-center collaboration of model training without sharing raw data.

In the context of medical image segmentation, although extensive research has been conducted on federated learning (Jiang et al., 2023; Sheller et al., 2019; Zhang et al., 2024; Luo et al., 2023), it is assumed that all the domains have sufficient labeled data, which is not practical in real-world scenarios. In practice, labeled data is often scarce and expensive to obtain in medical image segmentation tasks. To tackle this issue, some recent research has explored the combination of federated learning and semi-supervised segmentation, namely federated semi-supervised segmentation (FSSS) (Yang et al., 2021; Wu et al., 2024; Qiu et al., 2023; Ma et al., 2024b). FSSS aims to effectively utilize abundant unlabeled data from multiple domains to improve the model performance. Yang et al. (2021) was the pioneer in tackling FSSS for COVID-19 lesion segmentation, where they simply applied the centralized semi-supervised learning algorithm FixMatch (Sohn et al., 2020) to the federated setting. Wu et al. (2024) tried to improve the performance of FSSS by sharing prototypes among clients, causing potential privacy leakage. Qiu et al. (2023) proposed to apply Monte Carlo dropout to improve the reliability of pseudo label generation in FSSS, which puts extra computational burden on clients. Ma et al. (2024b) considered the scenario where each client holds different structures of local models, where their methods rely on the existence of a shared public dataset in the server, including potential risks of distributional mismatch between public and local datasets and concerns about data accessibility and fairness in real-world applications.

Another critical challenge in medical image segmentation is domain shift, caused by variations in data collected from different scanners, imaging protocols, or patient populations, which significantly impacts model generalization ability. To overcome the domain shift problem, domain generalization (DG) (Li et al., 2020a, 2018b) is introduced to learn models that can generalize well to unseen domains. In centralized learning, some recent research considered both domain shift and insufficient labeled data under the same framework, which they refer to as semi-supervised domain generalization (SemiDG) (Yao et al., 2022; Wang and Li, 2023; Liu et al., 2021d,c, 2022). Different from domain generalization (DG) (Li et al., 2020a, 2018b) that puts strong assumptions that all source domains have sufficient labeled data, SemiDG adopts the semi-supervised learning (SSL) paradigm and relaxes this assumption to a more practical scenario where very limited labeled data is available in each source domain while a large amount of data is unlabeled.

In FL, there are obvious difficulties in training a model that can generalize well to unseen domains in a distributed manner. Federated domain generalization (FedDG) (Liu et al., 2021a) is one emerging research area that considers the FL model's generalization ability on the unknown target client with domain shift. However, almost all aforementioned FSSS neglect the effect of this domain shift problem (Guan and Liu, 2021) that may cause suboptimal model aggregation and low effectivity of the utilization of unlabeled data, eventually leading to unsatisfactory generalization performance. Besides, the existing centralized SemiDG methods are not directly applicable to the federated setting due to their reliance on the utilization of multiple domains' data in a centralized manner.

Overall, these studies underscore the need for a new problem setting: domain generalized federated semi-supervised learning (FedSemiDG). This setting addresses a practical scenario in the healthcare domain, where multiple centers collaborate to train a model capable of generalizing to unseen domains in a distributed manner, despite having limited labeled data and abundant unlabeled data.

To tackle the domain shift problem in FSSL, several key challenges must be addressed: First, local models trained on diverse domains often exhibit varying levels of generalization, making it essential to design an effective aggregation strategy that ensures the global model achieves robust generalization. Second, high variances in training samples caused by domain shift may result in low-effectivity of the utilization of unlabeled data, especially for pseudo labeling-based methods (Sohn et al., 2020). Third, significant variations in image features across domains make learning generalized features in a distributed manner highly challenging, necessitating innovative and effective feature-learning strategies.

In this paper, we introduce the FedSemiDG problem setting and propose a novel framework Federated Generalization-Aware Semi-Supervised Learning (FGASL) to address this challenge by tackling key issues both globally and locally. On the server side, to mitigate the generalization difference among local models, we assess the generalization ability

of each local model by calculating the generalization gap between the local model and the global model on the local dataset. During the model aggregation process, we assign higher weights to local models with larger generalization gaps, aiming to enhance the global model's ability to generalize effectively to underrepresented data.

On the client side, considering that local models may drift away to client-specific knowledge during local training, we extend the classic teacher-student learning paradigm to a dual-teacher adaptive pseudo label refinement strategy to utilize both global generalized knowledge (static teacher) and local knowledge (dynamic teacher) in the pseudo label generation process. This design is inspired by Xu et al. (2024), who proposed leveraging unlabeled data from other centers to enhance the performance of models in a specific center under SSL, demonstrating that shared knowledge across centers can positively impact training. Specifically, the static teacher is a fixed version of the global model, providing better generalized knowledge, while the dynamic teacher, as a moving average of the local model, offers better local knowledge. By combining these two sources, the framework generates more reliable pseudo-labels. At the early stage of training, pseudo labels tend to be noisy due to poor calibration of neural networks (Guo et al., 2017). To address this, on top of the dual-teacher learning, we utilize a running uncertainty threshold to filter out the pseudo label with high uncertainty adaptively, which can effectively reduce the noise of pseudo labels and improve the quality of pseudo labels. Furthermore, to enhance robustness against domain-specific variations, we employ a perturbation-invariant alignment strategy. This approach mitigates the risk of overfitting to domain-specific features, ensuring that the model learns more generalized and transferable representations.

Overall, the main contributions of this paper are as follows:

1. **A novel problem setting:** We study a practical yet under-explored scenario in the healthcare domain, namely domain generalized federated semi-supervised learning (FedSemiDG), which aims to learn a model in a distributed manner from multiple domains with limited labeled data and abundant unlabeled data such that the model can generalize well to unseen domains.
2. **New insights:** We demonstrate that, under the FedSemiDG setting, either directly applying FSSL methods or simply combining FSSL and DG methods is insufficient to achieve satisfactory performance.
3. **New benchmarks:** We reimplemented various state-of-the-art FSSL and DG methods and evaluated them on three commonly used medical image segmentation datasets, which can serve as benchmarks for future research.
4. **A new framework:** We propose a novel framework FGASL for FedSemiDG, which tries to solve the domain shift problem in FSSL both globally and locally in three aspects: adaptive model aggregation to get a global model with better generalization ability, dual-teacher adaptive pseudo label refinement to acquire more reliable pseudo labels, and perturbation-invariant alignment to enhance robustness against domain-specific variations.

2. Related Work

2.1. Federated Learning

Although initially developed for mobile devices, federated learning (FL) has drawn great attention in healthcare due to its potential to enable multi-center collaboration and address the challenges of data privacy and security. FedAvg (McMahan et al., 2017) is one of the most popular algorithms for federated learning, which uses a weighted average of the local models to update the global model. The issues discussed in the FedAvg has been studied in recent works, such as the non-IID data distribution (Li et al., 2021b, 2020b; Gao et al., 2022; Li et al., 2021a), communication efficiency (Stich, 2018; Li et al., 2020c), privacy and security (Bonawitz et al., 2017; Geyer et al., 2017; Byali et al., 2020; Deng et al., 2024a).

In the field of medical imaging, FL has drawn increasing interest for allowing the creation of high-performing models from multiple data sources and maintaining privacy at the same time (Chen et al., 2022; Gurler and Rekik, 2022; Deng et al., 2024b; Elmas et al., 2022; Guan et al., 2024). A notable pilot study demonstrated the feasibility of FL for multi-site brain tumor segmentation (Sheller et al., 2019) without the need to share patient data. Since then, FL has shown great potential in various real-life medical imaging tasks. For instance, FL has been successfully applied to COVID-19 screening (Soltan et al., 2024), where clinical data from multiple hospitals were used to improve local model performance. Another example is detecting boundaries of rare cancers (Pati et al., 2022), where federated learning enabled significant improvement over a model trained on public datasets.

2.2. Domain Generalization & Federated Domain Generalization

Domain generalization (DG) is a challenging problem in machine learning, which aims to learn a model that can generalize well to unseen target domains without access to any of the target domain data. However, most existing DG

methods require access to multiple source domains during training (Li et al., 2019, 2018a; Xu et al., 2021a; Chen et al., 2024), which is often impractical in federated learning (FL) scenarios. Single-source domain generalization (Li et al., 2020a; Huang et al., 2020; Choi et al., 2023; Xu et al., 2021b; Wang et al., 2021) relaxes this requirement by requiring only a single source domain during training. For example, Xu et al. (2021b) applied Random Convolution (RC), consisting of a convolution layer randomly initialized for each mini-batch, to enable the model to learn generalizable visual representations by distorting local textures. Choi et al. (2023) extended RC to Progressive RC, which recursively stacks random convolution layers with a small kernel size instead of increasing the kernel size. In medical imaging, Li et al. (2020a) proposed learning domain-invariant features by encouraging distribution alignment and low-rank representation.

Nevertheless, there are limited studies addressing the DG problem in FL. Liu et al. (2021a) were the first to introduce the FedDG problem setting and proposed exchanging amplitude information in the frequency domain among clients to augment training data and improve performance. Similarly, Chen et al. (2023) proposed extracting and exchanging the overall domain style of local images among all clients. These early works require sharing information among clients, which could lead to potential privacy leakage. More recently, Zhang et al. (2023) introduced a variance reduction regularizer to the original global objective and proposed optimizing this objective by dynamically calibrating model aggregation weights, which is applicable only to fully labeled datasets. Le et al. (2024) presented a novel normalization method aimed at filtering out domain-specific features and applied a regularizer to encourage the model to capture domain-invariant representations.

2.3. Semi-supervised Segmentation & Semi-supervised Domain Generalization

Semi-supervised learning (SSL) is a well-established field with two main paradigms: consistency regularization (Miyato et al., 2018; Xie et al., 2020; Xu et al., 2023b) and pseudo-labeling (Sohn et al., 2020; Lee et al., 2013; Rizve et al., 2021). The basic idea of consistency regularization is to ensure that the model outputs consistent predictions (Sohn et al., 2020) or features (Abuduweili et al., 2021) for different views of the same input. Pseudo-labeling, on the other hand, generates either hard labels (Sohn et al., 2020) or soft labels (Tarvainen and Valpola, 2017) for unlabeled data during training. Due to the high cost of labeling, SSL has shown promising progress in medical image segmentation (Xu et al., 2022b; Bai et al., 2023; Xu et al., 2022a).

Moreover, there is growing concern about domain shift in SSL. For example, Bai et al. (2023) applied a bidirectional copy-paste strategy to alleviate the empirical mismatch problem between labeled and unlabeled data. Xu et al. (2024) proposed separated collaborative learning for semi-supervised prostate segmentation using multi-site unlabeled magnetic resonance imaging (MRI) data to introduce data heterogeneity. Ma et al. (2024a) referred to SSL with domain shift as mixed-domain semi-supervised medical image segmentation and designed a symmetric guidance training strategy and a random amplitude MixUp module.

Furthermore, semi-supervised domain generalization (SemiDG) is a new research area that addresses the domain shift problem in SSL. It focuses on a more practical and challenging scenario where the goal is to learn a model that generalizes well to unseen target domains. Early attempts leverage various techniques to address the SemiDG problem, such as meta-learning (Liu et al., 2021d) to simulate and handle domain shifts, Fourier transformation (Yao et al., 2022) to augment training data with cross-domain features, and compositionality to model robust features across domains (Liu et al., 2022). However, these methods are not directly applicable to federated settings because they rely on utilizing multiple domains' data in a centralized manner. In natural images, Zhou et al. (Zhou et al., 2023) applied style transfer to alter the appearance and texture of input images to enhance consistency learning, which may not be applicable to the medical domain due to the characteristics of medical images.

2.4. Federated Semi-supervised Learning

Unlike SSL, Federated Semi-supervised Learning (FSSL) (Jeong et al., 2021; Liang et al., 2022; Liu et al., 2024) integrates the advantages of FL and SSL, leveraging abundant unlabeled data from multiple distributed sources to reduce annotation burdens while simultaneously protecting data privacy, making it particularly attractive in the healthcare domain. For instance, Yang et al. (2021) applied FixMatch (Sohn et al., 2020) to generate pseudo labels for unlabeled data in COVID-19 lesion segmentation. Liu et al. (2021b) shared the disease relationship matrix among clients to enforce consistency regularization. Similarly, Wu et al. (2024) sought to improve the performance of FSSL by sharing prototypes among labeled and unlabeled clients to encourage the model to learn consistent features. However, sharing additional information among clients may pose risks of privacy leakage. Qiu et al. (2023) proposed to apply Monte Carlo dropout to improve the reliability of pseudo label generation in FSSS, which imposes

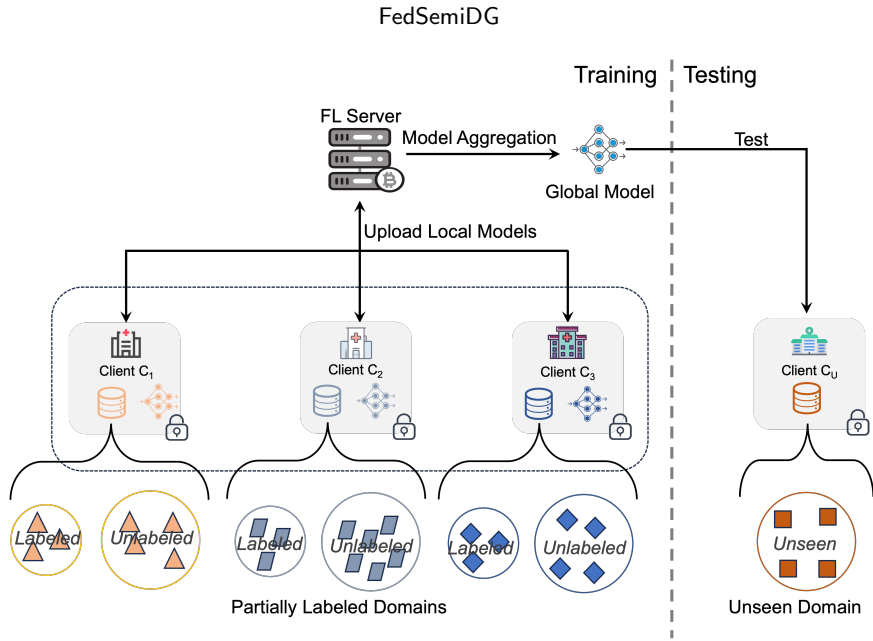


Figure 1: Illustration of domain generalized federated semi-supervised learning (FedSemiDG), where distributed domains collaboratively train a model to generalize to unseen domains.

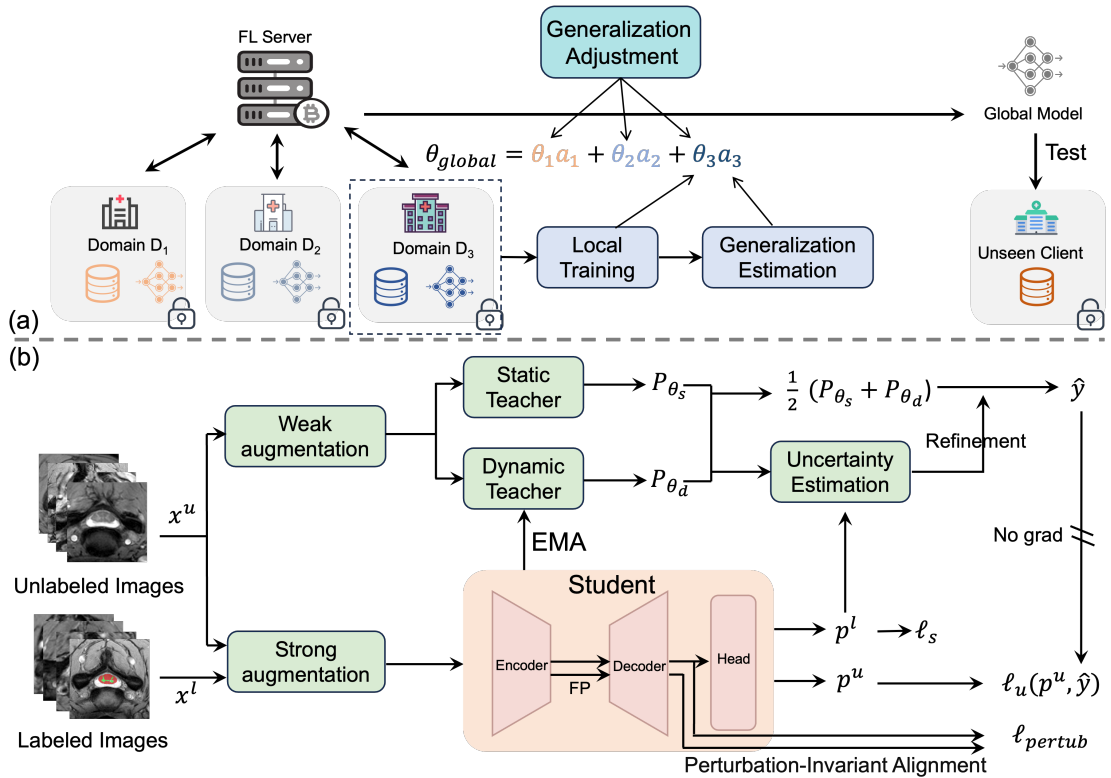


Figure 2: Illustration of the proposed framework Federated Generalization-Aware Semi-Supervised Learning (FGASL) for FedSemiDG scenario. The global model aggregation is enhanced by a generalization-aware weighting strategy, while local model training incorporates dual-teacher pseudo label refinement to acquire reliable pseudo labels and perturbation-invariant alignment through feature perturbation (FP) to ensure domain-invariant feature learning.

additional computational burdens on clients. Ma et al. (2024b) considered a scenario where each client holds differently structured local models. They introduced regularity condensation and regularity fusion to transfer autonomously selected knowledge to ensure personalization, which relies on a shared public dataset on the server. However, this method overlooks that not all tasks have a shared public dataset and that the distribution mismatch between public and local datasets raises potential fairness concerns in real-world applications.

Compared to existing FSSL works, our study broadens the scope of FSSL and is the first to introduce the Domain Generalized Federated Semi-Supervised Learning (FedSemiDG) problem setting. This extension is motivated by the observation that the domain shift problem has not been adequately considered or addressed in existing FSSL methods, both globally and locally.

3. Method

3.1. Problem Formulation and Framework Overview

In the FedSemiDG setting, as depicted in Fig. 1, we consider a central server that coordinates K participants, each holding data from a distinct source domain. Let $\{P^{(k)}(X, Y)\}_{k=1}^K$ denote K such joint distributions over the input space \mathcal{X} and the label space \mathcal{Y} . Each participant holds a local dataset D_k , consisting of a labeled subset $D_k^L = \{(x_k^l, y_k^l)\}_{i=1}^{N_k^L}$ with $(x_k^l, y_k^l) \sim P^{(k)}(X, Y)$, and an unlabeled subset $D_k^U = \{x_k^u\}_{i=1}^{N_k^U}$ where $x_k^u \sim P^{(k)}(X)$. We define $D_k = D_k^L \cup D_k^U$ as the union of the labeled and unlabeled data at the k -th participant. N_k^L and N_k^U are the numbers of labeled and unlabeled samples on the k -th participant, respectively. The goal of FedSemiDG is to learn a global model $f(x; \theta)$, parameterized by θ , that generalizes well to an unseen target domain \mathcal{T} with a distribution $P^*(X, Y)$ which differs from all source distributions $P^{(k)}$ for $k = 1, 2, \dots, K$.

Assuming $\mathcal{E}_{D_k}(\theta)$ is the local empirical risk minimization objective which incorporates both supervised and unsupervised components ℓ_s and ℓ_u balanced by a hyperparameter λ , and $\mathbf{a} = [a_1, a_2, \dots, a_K]$ are weights constrained by $\sum_{k=1}^K a_k = 1$ controlling the global optimization process. In FedAvg (McMahan et al., 2017), a_k is proportional to the number of samples in each domain; however, we consider a more general weighting strategy for flexibility. The global optimization problem reduces to the weighted expected risk:

$$\begin{aligned} \min_{\theta} \mathcal{E}_D(\theta) &= \sum_{k=1}^K a_k \mathcal{E}_{D_k}(\theta) \\ &= \sum_{k=1}^K a_k \left[\mathbb{E}_{(x^l, y^l) \sim \tilde{P}^{(k)}(X, Y)} [\ell_s(f(x^l; \theta), y^l)] + \lambda \mathbb{E}_{(x^u) \sim \tilde{P}^{(k)}(X)} [\ell_u(f(x^u; \theta))] \right]. \end{aligned} \quad (1)$$

As illustrated in Fig. 2, to address the FedSemiDG problem, we propose a novel framework FGASL comprising three key components: generalization-aware aggregation, dual-teacher adaptive pseudo label refinement, and perturbation-invariant alignment.

3.2. Generalization-Aware Aggregation

Due to the domain shift problem, local models trained on different domains may exhibit varied levels of generalization ability. Building on the approach proposed by Zhang et al. (2023), we reformulate the global optimization problem by incorporating the variance of generalization gaps $\{G_{D_k}(\theta)\}_{k=1}^K$ between local models and the global model on the local datasets, as shown below:

$$\min_{\theta} \mathcal{E}_D(\theta) = \sum_{k=1}^K a_k \mathcal{E}_{D_k}(\theta) + \beta \text{Var}(\{G_{D_k}(\theta)\}_{k=1}^K), \quad (2)$$

where β is a hyperparameter controlling the trade-off between the empirical risk and the variance of generalization gaps, and $\theta = \sum_{k=1}^K a_k \theta_k$ represents the global model parameter aggregated from all local models with weights \mathbf{a} .

In (2), $G_{D_k}(\theta)$ denotes the generalization gap on the local dataset D_k , where θ is the model parameter aggregated from all local models using weights \mathbf{a} . Given this connection, although we cannot optimize \mathbf{a} and θ_k simultaneously, we can instead optimize them iteratively. Specifically, θ_k is updated by minimizing the local empirical risk during local

training, after which the aggregation weights \mathbf{a} are optimized by reducing the variance of generalization gaps in the global model aggregation process.

Formally, the relationship between the global model parameter θ and the local model parameter θ_k can be rewritten as:

$$\theta = \sum_{k=1}^K a_k \theta_k = \theta_k + \sum_{i \neq k} a_i (\theta_i). \quad (3)$$

Intuitively, a larger generalization gap indicates lower generalization ability of the local model on its corresponding dataset, and vice versa. By assigning higher weights to local models with larger generalization gaps, we aim to improve the global model's generalization ability on underrepresented data.

Due to the limited amount of labeled data, the generalization gap cannot be directly measured by the error difference between the local model and the global model on the local dataset as in (Zhang et al., 2023). Instead, we propose using the output distribution discrepancy measured by the Kullback-Leibler (KL) divergence between the local model and the global model as a proxy for the generalization gap. Specifically, we define the generalization gap $G_{D_k}(\theta)$ as:

$$G_{D_k}(\theta) = \text{KL}(P_{\theta^r}(x|D_k) || P_{\theta_k^r}(x|D_k)), \quad (4)$$

where $P_{\theta^r}(x|D_k)$ and $P_{\theta_k^r}(x|D_k)$ are the output distributions of the initial global model and the updated local model on the local dataset D_k at the r -th FL round, respectively.

Increasing the weight a_k brings the global model closer to the local model θ_k , thereby reducing the generalization gap on the local dataset D_k . Consequently, the variance of generalization gaps $\text{Var}(G_{D_k}(\theta)_{k=1}^K)$ can be minimized by assigning higher weights to local models with larger generalization gaps. To achieve this, after local training in the r -th FL round, each participant first calculates the generalization gap $G_{D_k}(\theta)$ and sends it to the server along with the local model parameter θ_k . The server then minimizes the variance of generalization gaps by updating the aggregation weights \mathbf{a} using the following rule:

$$a_k^{r'} = \frac{(G_{\hat{D}_k}(\theta^r) - \mu) \cdot d^r}{\max_j (G_{\hat{D}_j}(\theta^r) - \mu)} + a_i^{r-1}, \quad a_k^r = \frac{a_k^{r'}}{\sum_{k=1}^K a_k^{r'}}, \quad (5)$$

where $\mu = \frac{1}{K} \sum_{k=1}^K G_{\hat{D}_k}(\theta^r)$ and $d^r = (1 - r/R) \cdot d$. Here, R denotes the total number of FL rounds, and d is a hyperparameter controlling the magnitude of the update, similar to β in (2). The initial weights a_i^0 are set to $1/K$ for all participants.

3.3. Dual-Teacher Adaptive Pseudo Label Refinement

Xu et al. (2023a) utilized the unlabeled data from other centers to support the training of a model in a specific center in SSL and showed promising results, which inspired us to design a dual-teacher adaptive pseudo label refinement strategy to utilize both global generalized knowledge (static teacher θ_s) and local knowledge (dynamic teacher θ_d) in the pseudo label generation process. Specifically, the static teacher is a fixed global model, while the dynamic teacher is initialized from the global model at each FL round and updated by exponential moving average (EMA) of the local model (student model) θ_k : $\theta_d = \pi_1 \theta_d + (1 - \pi_1) \theta_k$, where π_1 is the EMA decay rate. This design allows the static teacher to mitigate domain-specific drift in the dynamic teacher during local training, thereby producing more reliable pseudo labels.

To further enhance the robustness of pseudo labels, we adopt a weak-to-strong consistency learning paradigm (Sohn et al., 2020). For an unlabeled sample x , we first apply weak augmentation $\alpha(\cdot)$ and compute predictions from both teachers. The fused probability distribution is defined as:

$$P_f(c | \alpha(x)) = \frac{P_{\theta_s}(c | \alpha(x)) + P_{\theta_d}(c | \alpha(x))}{2}, \quad (6)$$

from which the pseudo-label is obtained as:

$$\hat{y} = \arg \max_c P_f(c | \alpha(x)). \quad (7)$$

To filter noisy pseudo labels, we compute an adaptive uncertainty threshold T_{un} based on labeled data. At each iteration, the entropy of labeled samples is calculated as $H(x^l) = -\sum_{c=1}^C P_{\theta_k}(c | x^l) \log(P_{\theta_k}(c | x^l) + \epsilon)$, and the threshold T_{lb} is set as the ramp-up quantile δ of these entropy values. The global threshold T_{un} is then updated via exponential smoothing with decay π_2 : $T_{un}^{(t)} = \pi_2 T_{un}^{(t-1)} + (1 - \pi_2) T_{lb}^{(t)}$. This ensures that the threshold dynamically adapts to the evolving model calibration and complexity during training.

Next, we apply strong augmentation $A(\cdot)$ to the unlabeled sample x to generate its counterpart $A(x)$ and compute the unlabeled loss l_u . For samples that pass the uncertainty threshold ($u_{s+d}(x) \leq T_{un}$), the consistency loss between weakly and strongly augmented views is defined as:

$$\ell_u = \frac{1}{B_u} \sum_{b=1}^{B_u} \mathbb{1}(u_{s+d}(x_b^u) \leq T_{un}) L(\hat{y}_b, P_{\theta_k}(y | A(x_b^u))), \quad (8)$$

where B_u is the batch size, and $L(\cdot)$ combines cross-entropy loss l_{ce} and Dice loss l_{dice} balanced by a hyperparameter η as $L(\cdot) = l_{ce} + \eta l_{dice}$. The uncertainty $u_{s+d}(x)$ combines entropy from both teachers:

$$u_{s+d}(x_b^u) = -\left[\sum_{c=1}^C P_{\theta_s}(c | \alpha(x_b^u)) \log(P_{\theta_s}(c | \alpha(x_b^u)) + \epsilon) + \sum_{c=1}^C P_{\theta_d}(c | \alpha(x_b^u)) \log(P_{\theta_d}(c | \alpha(x_b^u)) + \epsilon) \right] / 2. \quad (9)$$

This combination of dual-teacher refinement, uncertainty filtering, and consistency learning ensures that only high-quality pseudo labels contribute to model training, effectively leveraging unlabeled data to address domain shifts.

3.4. Perturbation-Invariant Alignment

Learning generalized features across multiple domains in a distributed manner is challenging and requires effective strategies. To improve robustness against domain-specific variations, we employ a simple-yet-effective perturbation-invariant alignment strategy. Formally, a segmentation model consists of an encoder E , a decoder D , and a classification head. We aim to encourage the model to learn features that are invariant to domain-specific perturbations. Specifically, we apply feature perturbations \mathcal{P} to the extracted features of the encoder $E(x)$, enforcing the decoder to generate consistent features for both original and perturbed inputs. The corresponding loss function is defined as:

$$\ell_{\text{perturb}} = \frac{1}{B_l} \sum_{b=1}^{B_l} \left\| D(E(x_b^l)) - D(E(\mathcal{P}(x_b^l))) \right\|_2^2 + \frac{1}{B_u} \sum_{b=1}^{B_u} \left\| D(E(x_b^u)) - D(E(\mathcal{P}(x_b^u))) \right\|_2^2, \quad (10)$$

where x_b^l and x_b^u represent labeled and unlabeled images within a batch, respectively; B_l and B_u denote the batch sizes for labeled and unlabeled data; \mathcal{P} is a perturbation function applied to the encoded features; E and D are the encoder and decoder of the segmentation model, respectively. In our experiments, we use channel dropout as the perturbation function. The loss encourages the decoder D to generate consistent outputs for the original and perturbed features, thereby promoting the encoder E to learn domain-invariant representations. More experimental analyses of various perturbation strategies are provided in Sec. 4.4.4.

The overall loss is: $l = \ell_s + \lambda_1 \ell_u + \lambda_2 \ell_{\text{perturb}}$, where supervised loss ℓ_s combines the cross-entropy loss and the Dice loss similar to the unsupervised loss ℓ_u , and ℓ_{perturb} is the perturbation-invariant alignment loss, λ_1 and λ_2 are hyperparameters that balance them.

4. Experiments

4.1. Datasets and Evaluation

4.1.1. Datasets

We evaluated our method on three real-world medical image segmentation tasks: cardiac MRI segmentation, spine MRI segmentation, and bladder cancer MRI segmentation.

Task 1: Cardiac MRI segmentation. The dataset (Campello et al., 2021) contains 320 subjects scanned by magnetic resonance scanners from four vendors (i.e., Siemens, Philips, GE, and Canon), primarily for the left ventricle (LV), left ventricle myocardium (MYO), and right ventricle (RV) segmentation tasks. Only the end-systole and end-diastole phases are annotated. The images were center-cropped and resized to 288×288 pixels.

Table 1
Dataset statistics across clients.

Dataset	Client 1		Client 2		Client 3		Client 4	
	Labeled	Unlabeled	Labeled	Unlabeled	Labeled	Unlabeled	Labeled	Unlabeled
Task 1: Cardiac	50	1478	50	1837	50	984	50	613
Task 2: Spine	30	350	30	186	30	339	30	236
Task 3: Bladder	50	815	50	315	50	105	50	139

Task 2: Spine MRI segmentation. The dataset (Perone et al., 2018) is collected from four different medical centers (University College London, Polytechnique Montreal, University of Zurich and Vanderbilt University) with different MRI systems (Philips Achieva, Siemens Trio and Siemens Skyra). The spinal cord and gray matter are annotated. The images were center-cropped and resized to 256×256 pixels.

Task 3: Bladder cancer MRI segmentation. The dataset (Cao et al., 2024) comprises 275 three-dimensional bladder T2-weighted MRI scans collected from four medical centers. Each scan provides diagnostic pathological labels for muscle invasion and pixel-level annotations of tumor contours. The images were center-cropped and resized to 160×160 pixels.

All tasks include **four** domains. The detailed statistics of the datasets are shown in Table 1. Each seen domain contains 50, 30, and 50 labeled slices for Task 1, Task 2, and Task 3, respectively. The labeled slices were selected randomly within each case, while ensuring no overlap with the unlabeled slices.

4.1.2. Evaluation

We followed the leave-one-domain-out evaluation protocol for all benchmarks as in (Liu et al., 2021a; Zhang et al., 2023; Le et al., 2024). Specifically, one domain was selected as the unseen target domain sequentially, while the remaining domains were used as source domains for training. We employed four commonly used evaluation metrics to evaluate the performance of segmentation, including Dice coefficient (DC), Jaccard coefficient (JC), the 95th percentile Hausdorff distance (HD95) and Average Surface Distance (ASD). All results were averaged over three independent runs.

4.2. Implementation Details

All the experiments were implemented using PyTorch, and all models were trained on an NVIDIA V100 GPU. For all three tasks, U-Net (Ronneberger et al., 2015) was used as the backbone for our method and for all compared methods. The network was optimized by Adam optimizer where the momentum terms were set to 0.9 and 0.99, with the learning rate set to 1×10^{-4} for Task 1 and Task 2, and 1×10^{-5} for Task 3. The batch size was 8 for both labeled and unlabeled data. The number of FL rounds was set to 100 and the number of local epochs was set to 1 for all tasks. The hyperparameters to control the trade-off of the loss functions were set to $\lambda_1 = 1.0$ for all tasks, $\lambda_2 = 0.3$ for Task 1 and Task 3, and $\lambda_2 = 0.5$ for Task 2. The EMA decay rate in student-teacher learning was set to $\pi_1 = 0.99$, while for global uncertainty threshold update, $\pi_2 = 0.9$ and the ramp-up quantile δ was gradually increased from 0.15 to 0.3 in Task 1 and Task 3, and from 0.1 to 0.5 in Task 2. By default, a channel dropout with 30% probability (`nn.Dropout2d()` in PyTorch) was adopted for Task 1 and Task 3, and 50% probability for Task 2 as our feature perturbation, which is inserted at the intersection of the encoder and decoder. For all tasks, weak data augmentation included random flip, rotation, translation, and scaling. Strong data augmentation included random contrast, brightness, and Gaussian blur.

4.3. Comparison with State-of-the-Art Methods

We compared our method with recent state-of-the-art (SOTA) FSSL methods, including RSCFed (Liang et al., 2022), DPL (Qiu et al., 2023), and FedCD (Liu et al., 2024). To further demonstrate the effectiveness of our approach, we also evaluated FedCD combined with single domain generalization (DG) techniques applicable to the FSSL setting, such as RC (Xu et al., 2021b) and LDDG (Li et al., 2020a). Additionally, we combined FedAvg (McMahan et al., 2017) with a SOTA semi-supervised learning (SSL) method, AugSeq (Zhao et al., 2023), and further incorporated RC and LDDG for comparison. Moreover, we included several baselines in our evaluation: the FL lower bound, represented by FedAvg with only labeled data; the FL upper bound, represented by FedAvg with fully labeled data; and local training baselines, either using only labeled data or leveraging FixMatch (Sohn et al., 2020).

Table 2

Comparison with the state-of-the-art methods on Task 1: Cardiac MRI Segmentation. The best and second-best results are highlighted in bold and underlined, respectively.

Task 1: LV / MYO / RV Segmentation													
Methods	#L	DC \uparrow				DC \uparrow		JC \uparrow		HD95 \downarrow		ASD \downarrow	
		Vendor A	Vendor B	Vendor C	Vendor D	Avg.	Avg.	Avg.	Avg.	Avg.	Avg.		
Local + LabelOnly	50	32.81/21.12/22.92	48.45/35.07/32.25	33.99/18.68/23.84	59.94/39.96/31.18	33.35	25.90	69.56	43.28				
Local + FixMatch (Sohn et al., 2020)	50	35.62/24.56/23.92	53.03/41.83/36.90	34.65/21.22/25.48	58.05/41.02/31.89	35.68	27.51	65.08	38.62				
FL lower bound	150	68.74/49.42/40.94	77.39/63.94/59.28	64.97/50.84/48.54	71.86/52.8/57.59	58.86	48.99	33.49	28.60				
RSCFed (Liang et al., 2022)	150	68.54/51.8/50.49	82.52/73.61/68.65	55.12/47.71/52.08	68.36/55.72/47.44	60.17	52.29	32.76	26.62				
DPL (Qiu et al., 2023)	150	63.88/56.26/44.65	48.86/31.09/17.57	44.41/33.48/35.93	63.88/56.26/44.65	40.16	30.58	40.73	26.09				
FedCD (Liu et al., 2024)	150	62.94/50.06/49.24	<u>83.12/74.91/69.61</u>	65.03/56.38/57.33	72.77/61.04/50.88	62.77	55.09	31.43	25.98				
+ RC (Xu et al., 2021b)	150	55.30/46.31/47.60	82.66/74.29/70.10	68.95/59.97/59.03	73.81/62.06/56.21	63.03	55.52	31.13	26.21				
+ LDDG (Li et al., 2020a)	150	52.23/35.29/27.51	81.41/74.19/71.62	67.90/56.27/51.45	43.79/29.17/20.36	50.93	43.13	44.65	30.78				
FedAvg (McMahan et al., 2017) + AugSeq (Zhao et al., 2023)	150	58.45/45.91/43.89	82.43/73.72/68.8	61.84/53.16/56.74	<u>79.6/67.28/63.30</u>	62.93	55.23	30.91	25.84				
+ RC (Xu et al., 2021b)	150	<u>66.53/54.6/49.93</u>	83.27/74.94/71.45	58.90/49.86/57.27	76.15/62.30/57.20	<u>63.53</u>	<u>56.22</u>	31.23	26.70				
+ LDDG (Li et al., 2020a)	150	58.98/47.43/45.86	70.02/56.85/47.70	61.65/49.74/44.59	61.42/41.20/30.90	51.36	42.47	46.14	29.73				
FGASL (ours)	150	72.82/60.56/55.92	82.08/74.18/70.76	<u>66.47/57.37/59.84</u>	80.51/68.46/62.25	67.60	59.76	26.65	21.86				
FL upper bound	*	85.07/72.56/64.31	89.42/82.29/74.58	88.58/80.36/76.88	89.42/81.65/80.88	80.50	72.25	13.09	9.92				

Table 3

Comparison with the state-of-the-art methods on Task 2: Spine MRI Segmentation. The best and second-best results are highlighted in bold and underlined, respectively.

Task 2: Spinal Cord / Grey Matter Segmentation													
Methods	#L	DC \uparrow				DC \uparrow		JC \uparrow		HD95 \downarrow		ASD \downarrow	
		Center A	Center B	Center C	Center D	Avg.	Avg.	Avg.	Avg.	Avg.	Avg.		
Local + LabelOnly	30	78.11/51.65	63.96/41.16	63.38/39.60	77.69/58.86	59.30	50.77	42.15	25.05				
Local + FixMatch (Sohn et al., 2020)	30	69.41/42.39	72.59/43.65	60.91/28.08	83.69/61.36	57.76	48.15	45.65	24.10				
FL lower bound	90	96.01/79.07	<u>90.00/71.71</u>	66.33/40.27	95.72/81.19	77.54	68.36	11.89	5.81				
RSCFed (Liang et al., 2022)	90	97.01/81.55	81.98/55.84	71.04/60.05	96.98/85.61	78.76	70.04	9.27	4.00				
DPL (Qiu et al., 2023)	90	93.06/63.15	14.47/3.21	20.98/4.03	90.28/65.71	44.36	36.20	79.91	42.69				
FedCD (Liu et al., 2024)	90	95.42/79.53	80.40/58.20	80.81/64.48	95.98/86.22	80.13	70.82	9.30	3.89				
+ RC (Xu et al., 2021b)	90	<u>96.12/80.37</u>	88.22/69.88	73.59/59.63	96.00/85.82	<u>81.20</u>	<u>72.49</u>	7.88	<u>3.46</u>				
+ LDDG (Li et al., 2020a)	90	93.60/77.02	86.65/53.56	78.48/56.55	94.90/80.83	77.65	67.62	10.75	3.79				
FedAvg (McMahan et al., 2017) + AugSeq (Zhao et al., 2023)	90	86.83/64.70	80.64/57.87	81.71/67.38	93.34/82.84	79.07	69.28	11.17	4.41				
+ RC (Xu et al., 2021b)	90	95.13/76.25	81.63/63.09	73.88/56.17	92.43/82.30	77.62	68.03	11.02	5.30				
+ LDDG (Li et al., 2020a)	90	93.60/77.02	79.77/53.57	72.26/58.68	94.85/75.02	77.69	67.53	12.13	5.30				
FGASL (ours)	90	95.48/79.86	95.59/80.68	82.08/66.70	<u>96.57/86.29</u>	85.41	77.04	4.99	1.96				
FL upper bound	*	96.48/81.82	94.27/80.51	85.29/68.54	98.38/86.92	86.23	77.85	7.15	2.44				

Across all three tasks, our method consistently showed significant improvements over the FL lower bound and outperformed existing SOTA approaches or their combinations with DG techniques in terms of average DC, JC, HD95, and ASD, as shown in Tables 2, 3, and 4. From the three tables, we can observe that FSSL only brings marginal improvements over the FL lower bound, indicating the challenges of learning from cross-domain data in the FSSL setting. Moreover, the DG techniques, such as RC and LDDG, can only slightly improve the performance or even degrade it in some cases. In contrast, our method achieved significant performance gains over the FL lower bound as well as existing SOTA methods. When compared with the second-best method, our approach achieves an improvement of 4.07%, 4.21%, and 2.93% in average DC on the Cardiac MRI, Spine MRI, and Bladder Cancer Segmentation tasks, respectively. We conducted paired t-tests to compare our method with the second-best performing approach in terms of average DC across all three tasks, and the p-value results ($p = 6.4 \times 10^{-3}$ in Task 1, $p = 5.3 \times 10^{-4}$ in Task 2, and $p = 3.0 \times 10^{-3}$ in Task 3) showed that our method significantly outperformed the second-best method with $p < 0.05$. Besides, as shown in Figs. 3 and 4, we provide qualitative comparisons on unseen domains in the Cardiac MRI, Spine MRI, and Bladder Cancer Segmentation tasks, where our method consistently achieved more accurate segmentation results compared to some top-performing approaches, demonstrating the robustness of our method in handling domain shift.

To further show that the FedSemiDG setting is clinically meaningful, we compared our method with the local training baselines. Localized training with SSL method FixMatch (Sohn et al., 2020) could not achieve satisfactory performance due to the lack of access to multi-center data. However, our approach showed substantial improvements, demonstrating the effectiveness of leveraging federated frameworks in multi-center collaborative learning. For instance,

Table 4

Comparison with the state-of-the-art methods on Task 3: Bladder Cancer Segmentation. The best and second-best results are highlighted in bold and underlined, respectively.

Task 3: Bladder Cancer Segmentation									
Methods	#L	DC \uparrow				DC \uparrow	JC \uparrow	HD95 \downarrow	ASD \downarrow
		Center 1	Center 2	Center 3	Center 4	Avg.	Avg.	Avg.	Avg.
Local + LabelOnly	50	48.13	50.97	55.46	54.97	52.38	39.76	44.85	17.00
Local + FixMatch (Sohn et al., 2020)	50	51.75	61.31	53.20	48.52	53.70	40.86	41.85	17.24
FL lower bound	150	58.36	56.28	60.55	57.75	58.23	44.55	58.24	21.85
RSCFed (Liang et al., 2022)	150	56.77	63.68	57.20	59.61	59.31	46.27	35.79	14.21
DPL (Qiu et al., 2023)	150	55.39	52.79	57.77	59.32	56.32	43.54	43.69	15.11
FedCD (Liu et al., 2024)	150	57.97	58.02	58.12	59.84	58.49	45.60	<u>33.44</u>	13.19
+ RC (Xu et al., 2021b)	150	60.30	54.69	61.65	59.89	59.13	<u>46.57</u>	41.44	13.83
+ LDDG (Li et al., 2020a)	150	54.80	63.86	59.08	58.46	59.05	46.15	33.79	<u>13.09</u>
FedAvg (McMahan et al., 2017) + AugSeq (Zhao et al., 2023)	90	<u>59.10</u>	54.12	61.14	60.83	58.80	45.84	44.42	15.69
+ RC (Xu et al., 2021b)	150	57.62	<u>65.29</u>	59.14	55.81	<u>59.47</u>	46.48	34.80	13.55
+ LDDG (Li et al., 2020a)	150	21.06	49.47	53.35	56.94	45.03	39.69	43.89	19.87
FGASL (ours)	150	59.10	67.63	62.53	<u>60.34</u>	62.40	49.18	33.21	12.13
FL upper bound	*	64.39	70.08	68.60	70.56	68.41	56.04	26.37	9.90

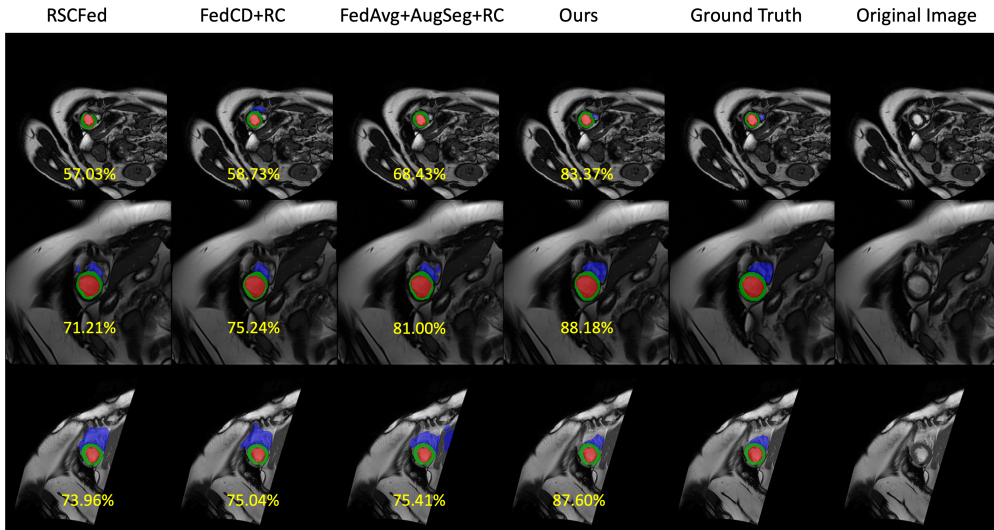


Figure 3: Exemplar cardiac MRI segmentation results on the unseen domain. The Dice scores (%) are displayed at the bottom.

our method improved Local+FixMatch by 31.92%, 27.65%, and 8.70% in average DC on the Cardiac MRI, Spine MRI, and Bladder Cancer Segmentation tasks, respectively. These results underscore the importance of collaborative learning across distributed clients, especially when labeled data is scarce.

4.4. Ablation Study

4.4.1. Effectiveness of Components

We conducted an ablation study to evaluate the effectiveness of each component in our proposed framework as shown in Table 5. We applied FixMatch (Sohn et al., 2020) as the SSL baseline and FedAvg (McMahan et al., 2017) as the FL model aggregation baseline. The introduction of the global aggregation-aware (GAA) component, dual-teacher refinement (DR), and perturbation-invariant alignment (PIA) individually improved the average Dice Coefficient (DC) by 2.37%, 1.89%, and 1.52%, respectively, with GAA being slightly more effective than the other two components. The results indicate that each component contributes to the overall performance improvement. Additionally, we assessed the performance of various two-component combinations. All combinations achieved better performance than the

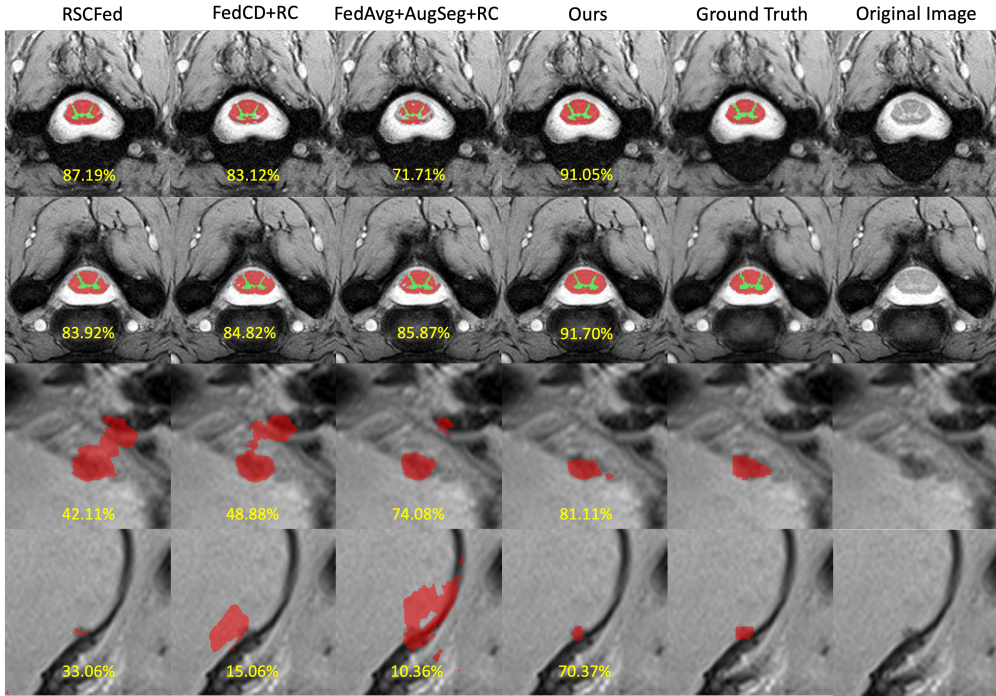


Figure 4: Exemplar segmentation on the unseen domain for spine (first and second rows), and bladder cancer (third and fourth rows). The Dice scores (%) are displayed at the bottom.

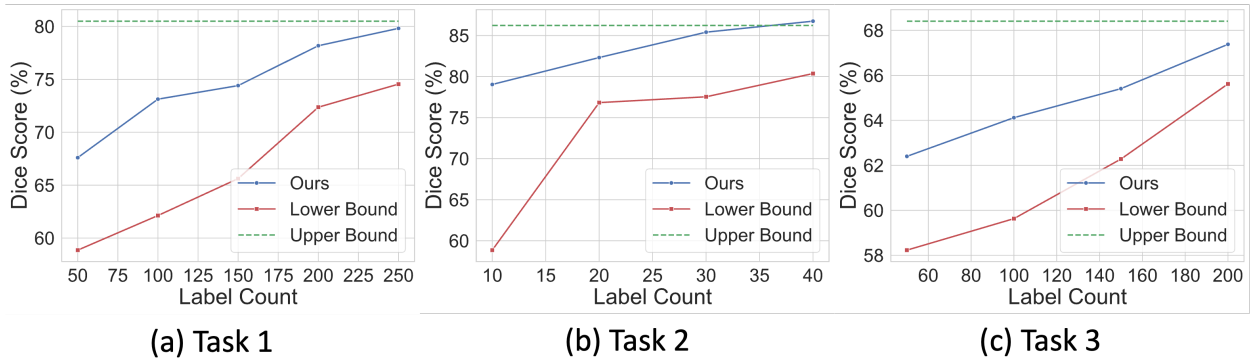


Figure 5: The relationship between the label count on each client and the average Dice score on Task 1: Cardiac MRI Segmentation, Task 2: Spine MRI Segmentation, and Task 3: Bladder Cancer Segmentation.

individual components, with the GAA and DR combination achieving slightly better results. Finally, integrating all three components yielded the best performance, achieving an average Dice score of 67.60%. These results highlight the importance of harmonizing global and local strategies within the FedSemiDG setting to achieve optimal outcomes.

4.4.2. Effect of Label Count on Performance

We performed a detailed analysis to examine how varying the label count in each domain, while ensuring it does not exceed the total number of labeled slices, impacts the performance of our method. The performance of our method ("Ours") is compared with the lower bound (FedAvg with only labeled data) and the upper bound (FedAvg with fully labeled data) on the three segmentation tasks. As shown in Fig. 5, as the label count increases, all tasks exhibit a clear trend of steady improvement in Dice score. The performance gap between our method and the lower bound remains significant, highlighting the effectiveness of our approach in mitigating label scarcity. And the close alignment with

Table 5

Ablation study on the effectiveness of each component in the proposed framework on Task 1: Cardiac MRI Segmentation. The best results are highlighted in bold.

GAA	DR	PIA	Avg. DC (%) \uparrow	Avg. JC (%) \uparrow	Avg. HD95 (mm) \downarrow	Avg. ASD (mm) \downarrow
			60.05	51.92	32.49	27.11
✓			62.37	52.31	31.55	26.78
	✓		61.89	51.67	30.72	25.93
		✓	61.52	52.03	31.60	26.82
✓	✓		64.92	56.33	29.91	24.09
✓		✓	65.72	57.19	30.22	25.67
	✓	✓	64.78	57.05	28.65	23.98
✓	✓	✓	67.60	59.76	26.65	21.86

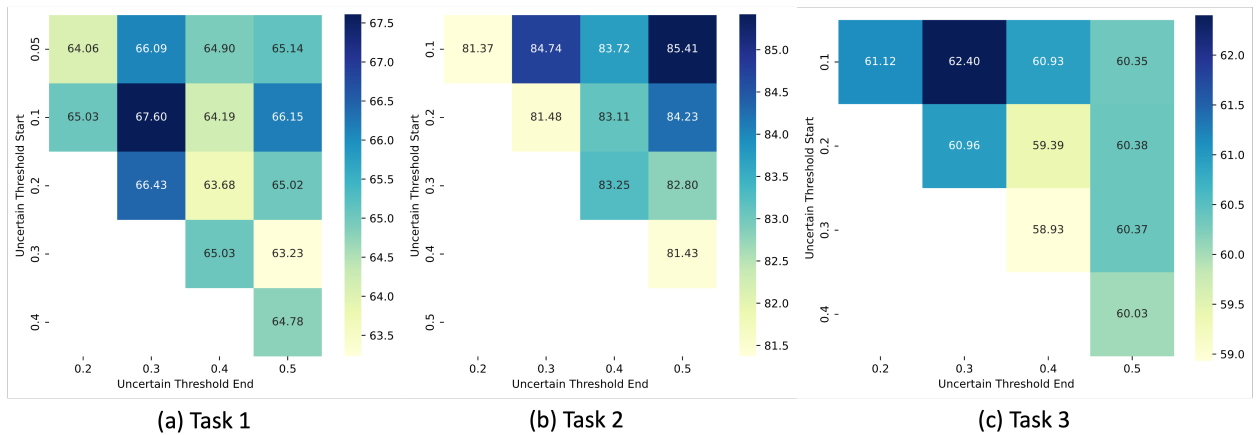


Figure 6: Hyperparameter analysis for the ramp-up quantile δ in the dual-teacher refinement on three segmentation tasks. δ is linearly increased from an initial value to a final value during the training process.

the upper bound further validates the capability of our method to achieve competitive performance even with limited labeled data. Additionally, as the label count achieves at certain levels, the performance of our method reaches the upper bound as seen in Task 1 and Task 3 or even surpasses it as seen in Task 2. These results emphasize that the proposed method is highly effective in utilizing labeled data, narrowing the performance gap to the upper bound while maintaining substantial improvements over the baseline lower bound.

4.4.3. Hyperparameter Analysis

We conducted a detailed hyperparameter analysis to evaluate the impact of two key components in our framework: the ramp-up quantile δ in the dual-teacher refinement process and the trade-off parameter λ_2 in the perturbation-invariant alignment loss combined with the feature dropout rate. These analyses, presented in Figs. 6 and 7, provide insights into the sensitivity of our framework to these hyperparameters and identify configurations that optimize performance across three segmentation tasks.

For the ramp-up quantile δ , we analyzed different combinations of starting and ending uncertainty thresholds. The results indicate that smaller starting values (0.1) paired with moderate ramp-up ranges (ending values of 0.3 to 0.4) consistently improve performance across tasks. This configuration balances the trade-off between exploiting confident predictions and refining uncertain ones during training, leading to stable and enhanced Dice scores.

In the analysis of the trade-off parameter λ_2 and the feature dropout rate, moderate values for both hyperparameters emerged as optimal. Specifically, setting λ_2 and the dropout rate to 0.3 resulted in the best performance for Task 1 and Task 3, while setting λ_2 and the dropout rate to 0.5 achieved the best performance for Task 2. Task 2 showed the most significant improvement under these settings, achieving a Dice core of 85.41%. These findings highlight the effectiveness of our method in leveraging perturbation-invariant alignment to improve generalization.

FedSemiDG

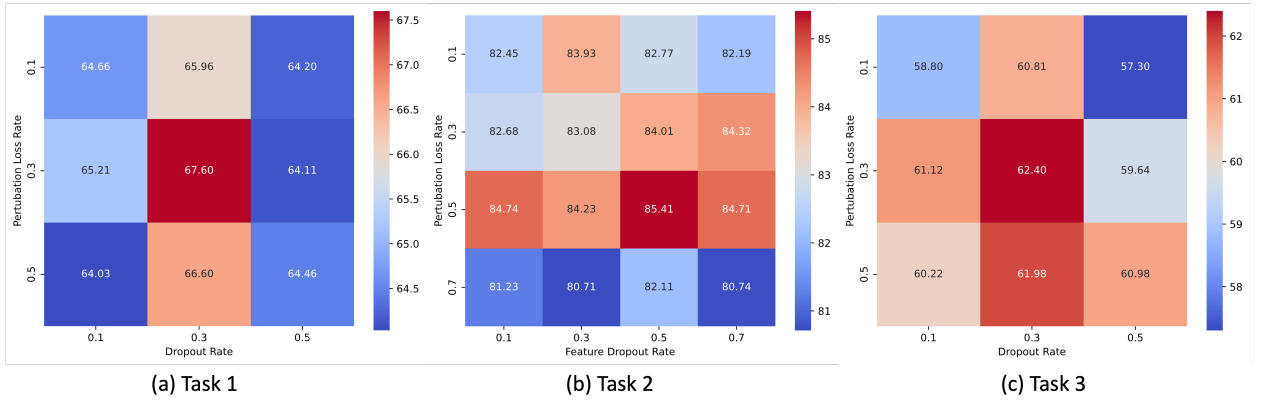


Figure 7: Hyperparameter analysis for the trade-off hyperparameter λ_2 in the perturbation-invariant alignment loss and dropout rate in the feature perturbation on three segmentation tasks.

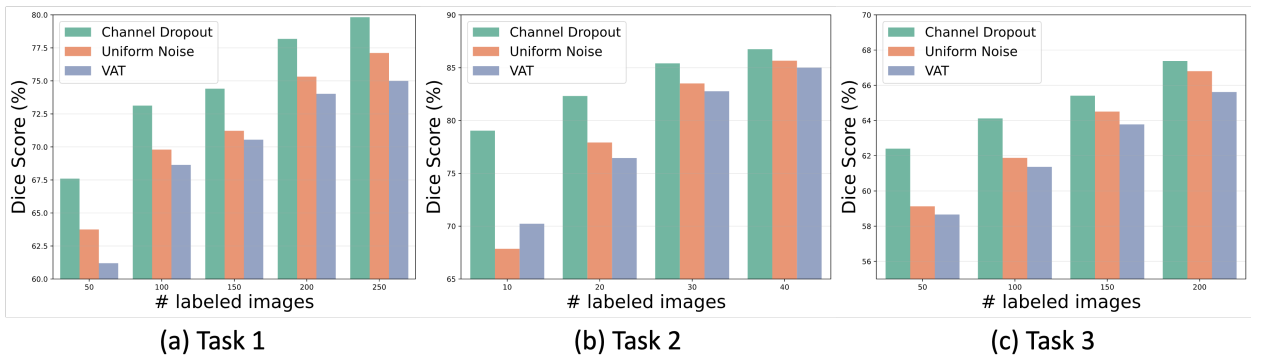


Figure 8: Ablation study on the efficacy of different feature perturbation strategies in our perturbation-invariant alignment component on three segmentation tasks.

Overall, these analyses emphasize the importance of careful hyperparameter tuning in maximizing the robustness and accuracy of our framework. The consistent trends across tasks suggest that the identified optimal ranges for δ , λ_2 , and dropout rate can serve as practical guidelines for similar segmentation tasks.

4.4.4. Ablation Study on Feature Perturbation Strategies

In our method, we utilize channel dropout as a straightforward and effective feature perturbation strategy. Alternative approaches, including uniform noise and virtual adversarial training (VAT) (Miyato et al., 2018), are also considered. To ensure a fair comparison, we adopt the hyperparameter settings outlined in (Ouali et al., 2020) for these strategies. Fig. 8 presents an ablation study evaluating the efficacy of different feature perturbation strategies in the perturbation-invariant alignment (PIA) component across three segmentation tasks, with performance measured using Dice Scores across varying numbers of labeled images.

Across all three tasks, channel dropout consistently achieves the highest performance regardless of the number of labeled images. Its advantage is most pronounced at lower label counts, where it significantly outperforms uniform noise and VAT. As the number of labeled images increases, the performance gap between channel dropout and the other methods narrows slightly but remains consistent. uniform noise shows competitive performance at higher label counts but falls short compared to channel dropout. VAT consistently performs the worst among the three strategies in all tasks. These results underline the effectiveness of channel dropout as a perturbation strategy within the PIA component. Its ability to introduce meaningful feature-level perturbations enhances generalization and segmentation accuracy across different tasks and label counts.

5. Discussion

Collecting large amounts of labeled medical data from a single center is inherently challenging, making Federated Semi-Supervised Learning (FSSL) an attractive solution for medical image segmentation tasks. Multi-center collaboration under the FSSL paradigm is critical for advancing medical image analysis, as it leverages diverse data from multiple sources and enables the development of robust models that generalize well, all while preserving data privacy. However, existing FSSL methods often overlook the pervasive issue of domain shifts in multi-center medical imaging data. Our work addressed this gap by introducing a novel framework tailored for Domain Generalized Federated Semi-Supervised Learning (FedSemiDG), a setting that has been underexplored yet is highly relevant to real-world medical imaging scenarios.

Technically, our experiments showed that previous FSSL methods only brought marginal improvements over the FL lower bound, while our approach demonstrated strong performance in this challenging scenario, demonstrating the effectiveness of our proposed framework. Clinically, FedSemiDG is particularly relevant for real-world multi-center medical imaging applications, where data is often scarce and domain shifts are prevalent. Our experiments show that local training could not achieve satisfactory performance due to the lack of access to multi-center data even with SSL methods, while our approach significantly improved the performance, showing great potential for clinical applications.

Despite the promising results of our proposed framework Federated Generalization-Aware Semi-Supervised Learning (FGASL) for FedSemiDG, our methods also involve more computational cost in generalization-aware aggregation, dual-teacher refinement, and perturbation-invariant alignment. Future work could explore lightweight aggregation and refinement strategies to reduce computational costs while maintaining performance. Extending the framework to address severe domain shifts and imbalanced datasets in other medical imaging tasks would also be valuable.

6. Conclusion

In this paper, we tackled the under-explored problem of FedSemiDG. Our proposed framework FGASL, which integrates global and local strategies, achieved robust generalization across unseen domains in challenging medical image segmentation tasks. These results highlighted the promise of FedSemiDG for advancing federated learning applications in healthcare.

References

- Abuduweili, A., Li, X., Shi, H., Xu, C.Z., Dou, D., 2021. Adaptive consistency regularization for semi-supervised transfer learning, in: Proceedings of the IEEE/CVF Conference on Computer Vision and Pattern Recognition, pp. 6923–6932.
- Bai, Y., Chen, D., Li, Q., Shen, W., Wang, Y., 2023. Bidirectional copy-paste for semi-supervised medical image segmentation, in: Proceedings of the IEEE/CVF Conference on Computer Vision and Pattern Recognition, pp. 11514–11524.
- Bonawitz, K., Ivanov, V., Kreuter, B., Marcedone, A., McMahan, H.B., Patel, S., Ramage, D., Segal, A., Seth, K., 2017. Practical secure aggregation for privacy-preserving machine learning, in: Proceedings of the 2017 ACM SIGSAC Conference on Computer and Communications Security, pp. 1175–1191.
- Byali, M., Chaudhari, H., Patra, A., Suresh, A., 2020. FLASH: Fast and robust framework for privacy-preserving machine learning. Proceedings on Privacy Enhancing Technologies .
- Campello, V.M., Gkontra, P., Izquierdo, C., Martin-Isla, C., Sojoudi, A., Full, P.M., Maier-Hein, K., Zhang, Y., He, Z., Ma, J., et al., 2021. Multi-centre, multi-vendor and multi-disease cardiac segmentation: the m&ms challenge. IEEE Trans. Med. Imaging 40, 3543–3554.
- Cao, K., Zou, Y., Zhang, C., Zhang, W., Zhang, J., Wang, G., Zhang, C., Lyu, J., Sun, Y., Zhang, H., et al., 2024. A multicenter bladder cancer mri dataset and baseline evaluation of federated learning in clinical application. Sci. Data 11, 1147.
- Chen, J., Jiang, M., Dou, Q., Chen, Q., 2023. Federated domain generalization for image recognition via cross-client style transfer, in: Proceedings of the IEEE/CVF Winter Conference on Applications of Computer Vision, pp. 361–370.
- Chen, K., Qin, T., Lee, V.H.F., Yan, H., Li, H., 2024. Learning robust shape regularization for generalizable medical image segmentation. IEEE Trans. Med. Imaging .
- Chen, Z., Yang, C., Zhu, M., Peng, Z., Yuan, Y., 2022. Personalized retrogress-resilient federated learning toward imbalanced medical data. IEEE Trans. Med. Imaging 41, 3663–3674.
- Choi, S., Das, D., Choi, S., Yang, S., Park, H., Yun, S., 2023. Progressive random convolutions for single domain generalization, in: Proceedings of the IEEE/CVF Conference on Computer Vision and Pattern Recognition, pp. 10312–10322.
- Deng, Z., Luo, L., Chen, H., 2024a. Enable the right to be forgotten with federated client unlearning in medical imaging, in: International Conference on Medical Image Computing and Computer Assisted Intervention, Springer. pp. 240–250.
- Deng, Z., Yang, Y., Suzuki, K., 2024b. Federated active learning framework for efficient annotation strategy in skin-lesion classification. J. Invest. Dermatol. In Press.
- Elmas, G., Dar, S.U.H., Korkmaz, Y., Ceyani, E., Susam, B., Ozbey, M., Avestimehr, S., Çukur, T., 2022. Federated learning of generative image priors for mri reconstruction. IEEE Trans. Med. Imaging 42, 1996–2009.

- Gao, L., Fu, H., Li, L., Chen, Y., Xu, M., Xu, C.Z., 2022. FedDC: Federated learning with non-IID data via local drift decoupling and correction, in: Proceedings of the IEEE/CVF Conference on Computer Vision and Pattern Recognition, pp. 10112–10121.
- Geyer, R.C., Klein, T., Nabi, M., 2017. Differentially private federated learning: A client level perspective. arXiv preprint arXiv:1712.07557.
- Guan, H., Liu, M., 2021. Domain adaptation for medical image analysis: a survey. IEEE Trans. Biomed. Eng. 69, 1173–1185.
- Guan, H., Yap, P.T., Bozoki, A., Liu, M., 2024. Federated learning for medical image analysis: A survey. Pattern Recognit., 110424.
- Guo, C., Pleiss, G., Sun, Y., Weinberger, K.Q., 2017. On calibration of modern neural networks, in: International Conference on Machine Learning, PMLR. pp. 1321–1330.
- Gurler, Z., Rekić, I., 2022. Federated brain graph evolution prediction using decentralized connectivity datasets with temporally-varying acquisitions. IEEE Trans. Med. Imaging 42.
- Huang, Z., Wang, H., Xing, E.P., Huang, D., 2020. Self-challenging improves cross-domain generalization, in: Proceedings of the European Conference on Computer Vision, Springer. pp. 124–140.
- Jeong, W., Yoon, J., Yang, E., Hwang, S.J., 2021. Federated semi-supervised learning with inter-client consistency & disjoint learning, in: 9th International Conference on Learning Representations (ICLR 2021).
- Jiang, M., Roth, H.R., Li, W., Yang, D., Zhao, C., Nath, V., Xu, D., Dou, Q., Xu, Z., 2023. Fair federated medical image segmentation via client contribution estimation, in: Proceedings of the IEEE/CVF Conference on Computer Vision and Pattern Recognition, pp. 16302–16311.
- Le, K., Ho, L., Do, C., Le-Phuoc, D., Wong, K.S., 2024. Efficiently assemble normalization layers and regularization for federated domain generalization, in: Proceedings of the IEEE/CVF Conference on Computer Vision and Pattern Recognition, pp. 6027–6036.
- Lee, D.H., et al., 2013. Pseudo-label: The simple and efficient semi-supervised learning method for deep neural networks, in: Workshop on Challenges in Representation Learning, ICML, Atlanta. p. 896.
- Li, D., Zhang, J., Yang, Y., Liu, C., Song, Y.Z., Hospedales, T.M., 2019. Episodic training for domain generalization, in: Proceedings of the IEEE/CVF International Conference on Computer Vision, pp. 1446–1455.
- Li, H., Pan, S.J., Wang, S., Kot, A.C., 2018a. Domain generalization with adversarial feature learning, in: Proceedings of the IEEE Conference on Computer Vision and Pattern Recognition, pp. 5400–5409.
- Li, H., Wang, Y., Wan, R., Wang, S., Li, T.Q., Kot, A., 2020a. Domain generalization for medical imaging classification with linear-dependency regularization. Advances in Neural Information Processing Systems 33, 3118–3129.
- Li, Q., He, B., Song, D., 2021a. Model-contrastive federated learning, in: Proceedings of the IEEE/CVF Conference on Computer Vision and Pattern Recognition, pp. 10713–10722.
- Li, T., Sahu, A.K., Zaheer, M., Sanjabi, M., Talwalkar, A., Smith, V., 2020b. Federated optimization in heterogeneous networks. Proceedings of Machine Learning and Systems 2, 429–450.
- Li, X., Huang, K., Yang, W., Wang, S., Zhang, Z., 2020c. On the convergence of FedAvg on non-IID data, in: International Conference on Learning Representations.
- Li, X., Jiang, M., Zhang, X., Kamp, M., Dou, Q., 2021b. Fedbn: Federated learning on non-iid features via local batch normalization, in: International Conference on Learning Representations.
- Li, Y., Tian, X., Gong, M., Liu, Y., Liu, T., Zhang, K., Tao, D., 2018b. Deep domain generalization via conditional invariant adversarial networks, in: Proceedings of the European Conference on Computer Vision, pp. 624–639.
- Liang, X., Lin, Y., Fu, H., Zhu, L., Li, X., 2022. RSCFed: Random sampling consensus federated semi-supervised learning, in: Proceedings of the IEEE/CVF Conference on Computer Vision and Pattern Recognition, pp. 10154–10163.
- Liu, Q., Chen, C., Qin, J., Dou, Q., Heng, P.A., 2021a. FedDG: Federated domain generalization on medical image segmentation via episodic learning in continuous frequency space, in: Proceedings of the IEEE/CVF Conference on Computer Vision and Pattern Recognition, pp. 1013–1023.
- Liu, Q., Yang, H., Dou, Q., Heng, P.A., 2021b. Federated semi-supervised medical image classification via inter-client relation matching, in: International Conference on Medical Image Computing and Computer Assisted Intervention, Springer. pp. 325–335.
- Liu, X., Thermos, S., Chatsias, A., O’Neil, A., Tsafaris, S.A., 2021c. Disentangled representations for domain-generalized cardiac segmentation, in: Statistical Atlases and Computational Models of the Heart. M&Ms and EMIDEC Challenges, Springer. pp. 187–195.
- Liu, X., Thermos, S., O’Neil, A., Tsafaris, S.A., 2021d. Semi-supervised meta-learning with disentanglement for domain-generalised medical image segmentation, in: International Conference on Medical Image Computing and Computer-Assisted Intervention, Springer. pp. 307–317.
- Liu, X., Thermos, S., Sanchez, P., O’Neil, A.Q., Tsafaris, S.A., 2022. vMFNet: Compositionality meets domain-generalised segmentation, in: International Conference on Medical Image Computing and Computer Assisted Intervention, Springer. pp. 704–714.
- Liu, Y., Wu, H., Qin, J., 2024. FedCD: Federated semi-supervised learning with class awareness balance via dual teachers, in: Proceedings of the AAAI Conference on Artificial Intelligence, pp. 3837–3845.
- Luo, G., Liu, T., Lu, J., Chen, X., Yu, L., Wu, J., Chen, D.Z., Cai, W., 2023. Influence of data distribution on federated learning performance in tumor segmentation. Radiol.: Artif. Intell. 5, e220082.
- Ma, Q., Zhang, J., Qi, L., Yu, Q., Shi, Y., Gao, Y., 2024a. Constructing and exploring intermediate domains in mixed domain semi-supervised medical image segmentation, in: Proceedings of the IEEE/CVF Conference on Computer Vision and Pattern Recognition, pp. 11642–11651.
- Ma, Y., Wang, J., Yang, J., Wang, L., 2024b. Model-heterogeneous semi-supervised federated learning for medical image segmentation. IEEE Trans. Med. Imaging.
- McMahan, B., Moore, E., Ramage, D., Hampson, S., y Arcas, B.A., 2017. Communication-efficient learning of deep networks from decentralized data, in: Artificial Intelligence and Statistics, PMLR. pp. 1273–1282.
- Miyato, T., Maeda, S.i., Koyama, M., Ishii, S., 2018. Virtual adversarial training: a regularization method for supervised and semi-supervised learning. IEEE Trans. Pattern Anal. Mach. Intell. 41, 1979–1993.
- Ouali, Y., Hudelot, C., Tami, M., 2020. Semi-supervised semantic segmentation with cross-consistency training, in: Proceedings of the IEEE/CVF Conference on Computer Vision and Pattern Recognition, pp. 12674–12684.
- Pati, S., Baid, U., Edwards, B., Sheller, M., Wang, S.H., Reina, G.A., Foley, P., Gruzdev, A., Karkada, D., Davatzikos, C., et al., 2022. Federated learning enables big data for rare cancer boundary detection. Nat. Commun. 13, 7346.

- Perone, C.S., Calabrese, E., Cohen-Adad, J., 2018. Spinal cord gray matter segmentation using deep dilated convolutions. *Sci. Rep.* 8, 5966.
- Qiu, L., Cheng, J., Gao, H., Xiong, W., Ren, H., 2023. Federated semi-supervised learning for medical image segmentation via pseudo-label denoising. *IEEE J. Biomed. Health. Inf.* 27, 4672–4683.
- Rizve, M.N., Duarte, K., Rawat, Y.S., Shah, M., 2021. In defense of pseudo-labeling: An uncertainty-aware pseudo-label selection framework for semi-supervised learning. *arXiv preprint arXiv:2101.06329*.
- Ronneberger, O., Fischer, P., Brox, T., 2015. U-Net: Convolutional networks for biomedical image segmentation, in: *International Conference on Medical Image Computing and Computer-Assisted Intervention*, Springer. pp. 234–241.
- Sheller, M.J., Reina, G.A., Edwards, B., Martin, J., Bakas, S., 2019. Multi-institutional deep learning modeling without sharing patient data: A feasibility study on brain tumor segmentation, in: *Brainlesion: Glioma, Multiple Sclerosis, Stroke and Traumatic Brain Injuries: 4th International Workshop, BrainLes 2018, Held in Conjunction with MICCAI 2018, Granada, Spain, September 16, 2018, Revised Selected Papers, Part I 4*, Springer. pp. 92–104.
- Sohn, K., Berthelot, D., Carlini, N., Zhang, Z., Zhang, H., Raffel, C., Cubuk, E., Kurakin, A., Li, C.L., 2020. FixMatch: simplifying semi-supervised learning with consistency and confidence, in: *Advances in Neural Information Processing Systems*, pp. 596–608.
- Soltan, A.A.S., Thakur, A., Yang, J., Chauhan, A., D’Cruz, L.G., Dickson, P., Soltan, M.A., Thickett, D.R., Eyre, D.W., Zhu, T., et al., 2024. A scalable federated learning solution for secondary care using low-cost microcomputing: Privacy-preserving development and evaluation of a COVID-19 screening test in UK hospitals. *Lancet Digit. Health* 6, e93–e104.
- Stich, S.U., 2018. Local SGD converges fast and communicates little, in: *International Conference on Learning Representations*.
- Tarvainen, A., Valpola, H., 2017. Mean teachers are better role models: Weight-averaged consistency targets improve semi-supervised deep learning results, in: *Advances in Neural Information Processing Systems*.
- Wang, H., Li, X., 2023. Towards generic semi-supervised framework for volumetric medical image segmentation, in: *Proceedings of the 37th International Conference on Neural Information Processing Systems*, pp. 1833–1848.
- Wang, Z., Luo, Y., Qiu, R., Huang, Z., Baktashmotlagh, M., 2021. Learning to diversify for single domain generalization, in: *Proceedings of the IEEE/CVF International Conference on Computer Vision*, pp. 834–843.
- Wu, H., Zhang, B., Chen, C., Qin, J., 2024. Federated semi-supervised medical image segmentation via prototype-based pseudo-labeling and contrastive learning. *IEEE Trans. Med. Imaging* 43, 649–661.
- Xie, Q., Dai, Z., Hovy, E., Luong, T., Le, Q., 2020. Unsupervised data augmentation for consistency training. *Advances in Neural Information Processing Systems* 33, 6256–6268.
- Xu, Q., Zhang, R., Zhang, Y., Wang, Y., Tian, Q., 2021a. A Fourier-based framework for domain generalization, in: *Proceedings of the IEEE/CVF Conference on Computer Vision and Pattern Recognition*, pp. 14383–14392.
- Xu, Z., Liu, D., Yang, J., Raffel, C., Niethammer, M., 2021b. Robust and generalizable visual representation learning via random convolutions, in: *International Conference on Learning Representations*.
- Xu, Z., Lu, D., Luo, J., Wang, Y., Yan, J., Ma, K., Zheng, Y., Tong, R.K.Y., 2022a. Anti-interference from noisy labels: Mean-teacher-assisted confident learning for medical image segmentation. *IEEE Trans. Med. Imaging* 41, 3062–3073.
- Xu, Z., Lu, D., Luo, J., Zheng, Y., Tong, R.K.y., 2024. Separated collaborative learning for semi-supervised prostate segmentation with multi-site heterogeneous unlabeled mri data. *Med. Image Anal.* 93, 103095.
- Xu, Z., Lu, D., Yan, J., Sun, J., Luo, J., Wei, D., Frisken, S., Li, Q., Zheng, Y., Tong, R.K.y., 2023a. Category-level regularized unlabeled-to-labeled learning for semi-supervised prostate segmentation with multi-site unlabeled data, in: *International Conference on Medical Image Computing and Computer Assisted Intervention*, Springer. pp. 3–13.
- Xu, Z., Wang, Y., Lu, D., Luo, X., Yan, J., Zheng, Y., Tong, R.K.y., 2023b. Ambiguity-selective consistency regularization for mean-teacher semi-supervised medical image segmentation. *Medical Image Analysis* 88, 102880.
- Xu, Z., Wang, Y., Lu, D., Yu, L., Yan, J., Luo, J., Ma, K., Zheng, Y., Tong, R.K.y., 2022b. All-around real label supervision: Cyclic prototype consistency learning for semi-supervised medical image segmentation. *IEEE Journal of Biomedical and Health Informatics* 26, 3174–3184.
- Yang, D., Xu, Z., Li, W., Myronenko, A., Roth, H.R., Harmon, S., Xu, S., Turkbey, B., Turkbey, E., Wang, X., 2021. Federated semi-supervised learning for COVID region segmentation in chest CT using multi-national data from China, Italy, Japan. *Med. Image Anal.* 70, 101992.
- Yao, H., Hu, X., Li, X., 2022. Enhancing pseudo label quality for semi-supervised domain-generalized medical image segmentation, in: *Proceedings of the AAAI Conference on Artificial Intelligence*, pp. 3099–3107.
- Zhang, F., Liu, H., Cai, Q., Feng, C.M., Wang, B., Wang, S., Dong, J., Zhang, D., 2024. Federated cross-incremental self-supervised learning for medical image segmentation. *IEEE Trans. Neural Netw.*
- Zhang, R., Xu, Q., Yao, J., Zhang, Y., Tian, Q., Wang, Y., 2023. Federated domain generalization with generalization adjustment, in: *Proceedings of the IEEE/CVF Conference on Computer Vision and Pattern Recognition*, pp. 3954–3963.
- Zhao, Z., Yang, L., Long, S., Pi, J., Zhou, L., Wang, J., 2023. Augmentation matters: A simple-yet-effective approach to semi-supervised semantic segmentation, in: *Proceedings of the IEEE/CVF Conference on Computer Vision and Pattern Recognition*, pp. 11350–11359.
- Zhou, K., Loy, C.C., Liu, Z., 2023. Semi-supervised domain generalization with stochastic stylematch, in: *International Journal of Computer Vision*, Springer. pp. 2377–2387.